

An Algorithm for Cellular Reprogramming

Scott Ronquist¹, Geoff Patterson², Markus Brown³, Stephen Lindsly¹, Haiming Chen¹, Lindsey A. Muir⁴, Max Wicha⁵, Anthony Bloch⁶, Roger Brockett⁷, and Indika Rajapakse^{1,4,8}

¹Department of Computational Medicine and Bioinformatics, Medical School, University of Michigan, Ann Arbor, MI 48109

²IXL Learning, Raleigh, NC 27560

³Department of Biological Sciences, University of Maryland, College Park

⁴Department of Pediatrics and Communicable Diseases, University of Michigan, Ann Arbor, MI 48109

⁵Department of Hematology/Oncology, University of Michigan, Ann Arbor, MI 48109

⁶Department of Mathematics, University of Michigan, Ann Arbor, MI 48109

⁷Harvard School of Engineering and Applied Sciences, Cambridge, MA 02138

⁸Corresponding author: indikar@umich.edu

Abstract

The day we understand the time evolution of subcellular elements at a level of detail comparable to physical systems governed by Newton's laws of motion seems far away. Even so, quantitative approaches to cellular dynamics add to our understanding of cell biology, providing data-guided frameworks that allow us to develop better predictions about, and methods for, control over specific biological processes and system-wide cell behavior. In this paper, we describe an approach to optimizing the use of transcription factors (TFs) in the context of cellular reprogramming. We construct an approximate model for the natural evolution of a cell cycle synchronized population of human fibroblasts, based on data obtained by sampling the expression of 22,083 genes at several time points along the cell cycle. In order to arrive at a model of moderate complexity, we cluster gene expression based on the division of the genome into topologically associating domains (TADs) and then model the dynamics of the TAD expression levels. Based on this dynamical model and known bioinformatics, such as transcription factor binding sites (TFBS) and functions, we develop a methodology for identifying the top transcription factor candidates for a specific cellular reprogramming task. The approach used is based on a device commonly used in optimal control. Our data-guided methodology identifies a number of transcription factors previously validated for reprogramming and/or natural differentiation. Our findings highlight the immense potential of dynamical models, mathematics, and data-guided methodologies for improving strategies for control over biological processes.

Significance Statement

Reprogramming the human genome toward any desirable state is within reach; application of select transcription factors drives cell types toward different lineages in many settings. We introduce the concept of data-guided control in building a universal algorithm for directly reprogramming any human cell type into any other type. Our algorithm is based on time series genome transcription and architecture data and known regulatory activities of transcription factors, with natural dimension reduction using genome architectural features. Our algorithm predicts known reprogramming factors, top candidates for new settings, and ideal timing for application of transcription factors. This framework can be used to develop strategies for tissue regeneration, cancer cell reprogramming, and control of dynamical systems beyond cell biology.

Introduction

In 1989, pioneering work by Weintraub *et al.* successfully reprogrammed human fibroblast cells to muscle cells via over-expression of transcription factor (TF) MYOD1, becoming the first to demonstrate that the natural course of cell development could be altered [1]. In 2007, Yamanaka

et al. changed the paradigm further by successfully reprogramming human fibroblast cells to an embryonic-stem-cell-like state (induced pluripotent stem cells; iPSCs) using four TFs: POU5F1, SOX2, KLF4, MYC. This showed that a differentiated cell state could be reverted to a more pluripotent state [2].

These remarkable findings demonstrated that the genome is a system capable of being controlled via an external input of TFs. In this context, determining how to push the cell from one state to another is, at least conceptually, a classical problem of control theory [3]. The difficulty arises in the fact that the dynamics – and even proper representations of the cell state and inputs – are not well-defined in the context of cellular reprogramming. Nevertheless, it seems natural to treat reprogramming as a problem in control theory, with the final state being the desired reprogrammed cell. In this paper, we provide a control theoretic framework based on empirical data and demonstrate the potential of this framework to provide novel insights into cellular reprogramming [4, 5].

Our goal is to mathematically identify TFs that can directly reprogram human fibroblasts to a desired target cell type. As part of our methodology, we create a model for the natural dynamics of proliferating human fibroblasts. We couple data from bioinformatics with methods of mathematical control theory—a framework which we dub *data-guided control* (DGC). Using time series data and a natural dimension reduction through topologically associating domains (TADs), we capture the natural dynamics of the cell, including the cell cycle.

We use this model to determine a principled way to identify the best TFs for efficient reprogramming of a given cell type toward a desired target cell type. Previously, selection of TFs for reprogramming has been based largely on trial and error, typically relying on TF differential expression between cell types for initial predictions. Recently, Rackham *et al.* devised a predictive method based on differential expression as well as gene and protein network data [6]. Our approach is fundamentally different in that we take a dynamical systems point of view, opening avenues for investigating efficiency (probability of conversion), timing (when to introduce TFs), and optimality (minimizing the number of TFs and amount of input).

Using genomic transcription and architecture data, our method identifies TFs previously found to reprogram human fibroblasts into embryonic stem cell-like cells and reprogram fibroblasts into muscle cells. Our method also predicts TFs for conversion between human fibroblasts and many additional target cell types. In addition, we show the efficacy of using TADs for genome dimension reduction. Our analysis predicts the points in the cell cycle at which the insertion of TFs can most efficiently affect a desired change of cell state. Implicit in this approach is the notion of distance between cell types, which is measured in terms of the amount of transcriptional change required to transform one cell type into another. In this way, we are able to provide a comprehensive quantitative view of human cell types based on the respective distances between cell types.

Our framework separates into three parts:

1. **Define the state.** Use structure and function observations of the initial and target cell types' genomes to define a comprehensive state representation.
2. **Model the dynamics.** Apply model identification methods to approximate the natural dynamics of the genome, from time series data.
3. **Define and evaluate the inputs.** Infer from bioinformatics (TF binding location and function) where TFs can influence the genome, then quantify controllability properties with respect to the target cell type.

The actual dynamics of the genome are undoubtedly very complicated, but as is often done in mathematical modeling studies, we use measurements to identify a linear approximation. This will take the form of a difference equation that is widely studied in the control systems literature, [7]

$$x_{k+1} = A_k x_k + B u_k. \quad (1)$$

In this case, the three items listed above correspond respectively to the value of the state x_k at time k , the time dependent state transition matrix A_k , and the input matrix B (along with the input function u_k).

Methods

Genome State Representation and Dimension Reduction: x_k

The state representation x in Eq. 1 is the foundation for any control system and is critical for controllability analysis. To fully represent the state of a cell, a high number of measurements would need to be taken, including gene expression, protein level, chromatin conformation, and epigenetic measurements. As an initial simplification, we assume that the gene expression profile is a sufficient representation of the cell state.

Gene expression for a given cell is dependent on a number of factors, including (but not limited to): cell type, cell cycle stage, circadian rhythm stage, and growth conditions. In order to best capture the natural fibroblast dynamics from population-level data, time series RNA-seq was performed on cells that were cell cycle and circadian rhythm synchronized in normal growth medium conditions (See SI). Prior to data collection, all cells were temporarily held in the first stage of the cell cycle, G_0/G_1 , via serum starvation. Upon release into the cell cycle, the population was observed every $\Delta t = 8$ hours (h) for 56 h, yielding 8 time points (at 0, 8, 16, ..., 56 h). Let $g_{i,k}$ be the measured activity of gene $i = 1, \dots, N$ at measurement time $k = 1, \dots, 8$, where N is the total number of human genes observed (22,083). Analysis of cell-cycle marker genes indicated that the synchronized fibroblasts took between 32-40 h to complete one cell cycle post growth medium introduction, after which cells became largely unsynchronized (Fig. S1). Because of this, we define $K = 5$ to be the total number of time points used for this model.

An obstacle to using g to represent x in a dynamical systems approach is the computational feasibility of studying a system with over 20,000 variables, necessitating a dimension reduction. Naïve dimension reductions such as partitioning the genome into 1 mega-base pair (Mb) bins ignores inherent structural organization of the genome and obscures important intricacies of finer resolutions. A comprehensive genome state representation should include aspects of both structure and function, and simultaneously have low enough dimension to be computationally reasonable. Along these lines, we propose a biologically inspired dimension reduction based on topologically associated domains (TADs).

The advent of genome-wide chromosome conformation capture (Hi-C) allowed for the studying of higher order chromatin structure and the subsequent discovery of TADs [8]. TADs are inherent structural units of chromosomes: contiguous segments of the 1-D genome for which empirical physical interactions can be observed [9]. Moreover, genes within a TAD tend to exhibit similar activity, and TAD boundaries have been found to be largely cell-type invariant [9, 10, 11]. TADs group structurally and functionally similar genes, serving as a natural dimension reduction that preserves important genomic properties. Fig. 1 depicts an overview of this concept. We computed TAD boundaries from Hi-C data via an algorithm that uses Fiedler vector partitioning, described in Chen *et al.* (See SI) [12].

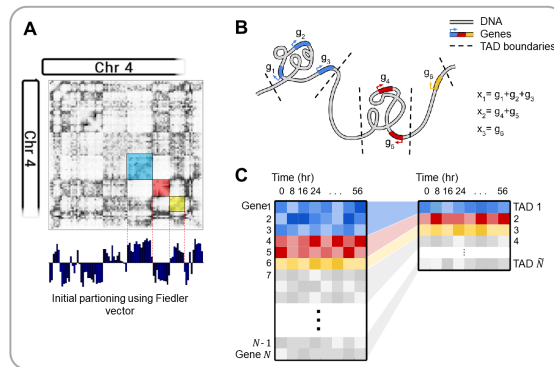


Figure 1: Overview of TAD dimension reduction. (A) Partitioning the Hi-C matrix based on the Fiedler vector. (B) Cartoon depiction of TAD genomic structure. (C) TAD dimension reduction summary.

Let $tad(i) := j$ if gene i is contained within TAD j . We define each state variable $x_{j,k}$ to be the expression level of TAD $j = 1, \dots, \tilde{N}$ at time k , where $\tilde{N} = 2,245$ is the total number of TADs that contain genes. Specifically, $x_{j,k}$ is defined as the sum of the expression levels of all genes within

the TAD, measured in reads per kilobase of transcript per million (RPKM), i.e.

$$x_{j,k} := \sum_{\substack{i \text{ s.t.} \\ \text{tad}(i)=j}} g_{i,k}. \quad (2)$$

The vector of all TAD activities at measurement k is denoted with a single subscript $x_k \in \mathbb{R}^{\tilde{N} \times 1}$, $k = 1, \dots, K$.

State Transition Matrix: A_k

Given the data we have, perhaps the most direct way to model the evolution of TAD activity level would be to assume a model of the form $x_{k+1} = x_k + y$, where x_k and x_{k+1} come from data, and y is the vector difference of x_{k+1} and x_k . However, the data could also be viewed in a different way. Taken over a full cycle, the average value of the expression level of the 2,245 TADs is known, within experimental error. Assuming that there is a function f which maps x_k to x_{k+1} , we can subtract the steady state average, \bar{x} , and focus on measuring the deviation from average as the cycle evolves. With this in mind, we have $f(x) = \bar{x} + A(x - \bar{x})$ where A is allowed to depend on x 's location in the cell cycle. That is, we build a model for the variation of the cell cycle about \bar{x} . For the model to match data and capture variability over the cell cycle, we will need to have a different A for each time step. Using the principle that A should differ as little from the identity as possible, we let A_k be the identity plus a rank one matrix chosen to match the data, for each time step k . In this case we have $x_{k+1} - \bar{x} = A_k(x_k - \bar{x})$.

We define a time dependent state transition matrix A_k .

$$A_k := I_{\tilde{N}} + \frac{(x_{k+1} - x_k)x_k^\top}{x_k^\top x_k} \in \mathbb{R}^{\tilde{N} \times \tilde{N}}, \quad k = 1, 2, 3, 4, 5 \quad (3)$$

where $I_{\tilde{N}}$ is the $\tilde{N} \times \tilde{N}$ identity matrix.

Input Matrix and Input Signal: B, u_k

With the natural TAD-level dynamics established in the context of our control Eq. 1, we turn our attention to quantifying methods for control.

A TF is a protein that can regulate a gene positively or negatively by binding to a specific DNA sequence near a gene and encouraging or discouraging transcription. This is accomplished, for example, by altering local chromatin conformation or by recruiting RNA polymerase II and other transcriptional machinery [13]. The degree to which a TF activates or represses a gene depends on the specific TF-gene interaction and most likely on a variety of nuclear subtleties and intricacies that are difficult to quantify. Let $w_{i,m}$ be the theoretical *regulation weight* of TF m on gene i , where $w_{i,m} > 0$ ($w_{i,m} < 0$) if TF m activates (represses) gene i , and $m = 1, \dots, M$, where M is the total number of well-characterized TFs. Weights that are bigger in absolute value, $|w_{i,m}| \gg 0$, indicate stronger transcriptional influence, and weights equal to zero, $w_{i,m} = 0$, indicate no influence.

Extensive TF perturbation experiments would be needed to determine $w_{i,m}$ for each TF m on each gene i . Instead, we propose an alternative (simplified) method to approximate $w_{i,m}$ from existing, publicly available data for TF binding sites, gene accessibility, and average activator/repressor activity. To determine the number of possible binding sites a TF m recognizes near gene i , we scanned the reference genome for the locations of potential TF binding sites (TFBSs) (See SI). Position frequency matrices (PFMs), which give information on TF-DNA binding probability, were obtained for 547 TFs from a number of publicly available sources ($\therefore M = 547$). Let $c_{i,m}$ be the number of TF m TFBSs found within $\pm 5\text{kb}$ of the transcriptional start site (TSS) of gene i (Fig. S2). In our model, the magnitude of $w_{i,m}$ is proportional to $c_{i,m}$. False negatives would include distal TFBSs outside of the $\pm 5\text{kb}$ window, while false positives would be erroneous TFBS matches.

Although many TFs can do both in the right circumstances, most TFs have tendency toward either activator or repressor activity [13]. That is, if TF m is known to activate (repress) most genes, we can say with some confidence that TF m is an activator (repressor), so $w_{i,m} \geq 0$ ($w_{i,m} \leq 0$) for all i . To determine a TF's function, we performed a literature search for all 547 TFs and labeled 299 as activators and 124 as repressors (See SI). The remaining TFs were labeled unknown for lack of conclusive evidence for activator or repressor function. In the case of inconclusive evidence, the

TF was evaluated as both an activator and a repressor in separate calculations. Here, we define a_m as the activity of TF m , with 1 and -1 denoting activator and repressor, respectively, and the sign of $w_{i,m}$ will be determined by a_m .

TFBSs are cell-type invariant since they are based strictly on the linear genome. However, it is known that for a given cell type, certain areas of the genome may be opened or closed depending on epigenetic aspects. To capture cell type specific regulatory information, we obtained gene accessibility data through DNase-seq. DNase-seq extracts cell type specific chromatin accessibility information genome-wide by testing the genome’s sensitivity to the endonuclease DNase I, and sequencing the non-digested genome fragments. This data is used for our initial cell type to determine which genes are available to be controlled by TFs [14]. Here, we define s_i be the DNase I sensitivity information (accessibility; open/close) of gene i in the initial state, with 1 and 0 denoting accessible and inaccessible, respectively (See SI).

We approximate $w_{i,m}$ as

$$w_{i,m} := a_m s_i c_{i,m}, \quad (4)$$

so that the magnitude of influence is equal to the number of observed consensus motifs $c_{i,m}$, except when the gene is inaccessible ($s_i = 0$) in which case $w_{i,m} = 0$.

Since we are working off a TAD-dimensional model, our input matrix B must match this dimension. Let b_m be a 2,245-dimensional vector, where the j^{th} component is

$$b_{j,m} := \sum_{\substack{i \text{ s.t.} \\ \text{tad}(i)=j}} w_{i,m} \quad (5)$$

and define a matrix $B = [b_1 \ b_2 \ \dots \ b_M]$.

The amount of control input is captured in u_k , which is a $\mathbb{R}^{M \times 1}$ vector representing the quantity of the external TFs we are inputting to the system (cell) at time k . This can be controlled by the researcher experimentally through manipulation of the TF concentration [15]. In this light, we restrict our analysis to $u_k \geq 0$ for all k , as TFs cannot be subtracted from the cell. $u_{m,k}$ is defined as the amount of TF m to be added at time point k .

With all variables of our control Eq. 1 defined, we can now attempt to predict which TFs will most efficiently achieve cellular reprogramming from some x_I (initial state; fibroblast in our setting) to x_T (target state; any human cell type for which compatible RNA-seq data is available) through manipulation of u_k . An overview of our DGC framework is given in Fig. 2.

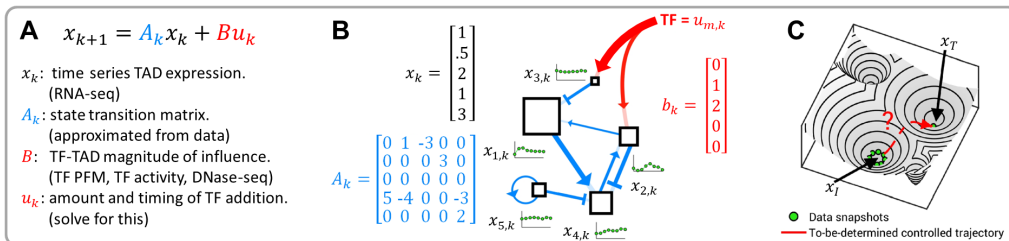


Figure 2: Data-guided control overview. (A) Summary of control equation variables. (B) Each TAD is a node in a dynamic network. The blue connections represent the edges of the network and are determined from time series fibroblast RNA-seq data. The miniature green plots represent the expression of each TAD changing over time. The red arrows indicate additional regulation imposed by exogenous transcription factors. (C) A conceptual illustration of the problem: can we determine transcription factors to push the cell state from one basin to another?

Selection of TFs

We consider different scenarios for the type of input regime. The first is assuming the input signal is constant $u_1 = u_k = \bar{u}$, intended to mimic empirical regimes where TFs are given at a single time point. We will show that this method is theoretically inferior to inputting different TFs at different points in the cell cycle in a later section.

Eq. 1 has an explicit solution that is easily computed.

$$\begin{aligned}x_2 &= A_1 x_1 + B u_1 \\x_3 &= A_2 A_1 x_1 + A_2 B u_1 + B u_2 \\x_4 &= A_3 A_2 A_1 x_1 + A_3 A_2 B u_1 + A_3 B u_2 + B u_3 \\&\vdots\end{aligned}$$

Notice the expression for x_4 depends the input matrix B and the input signal u_k .

If x_T is a target condition, then the Euclidean distance $\|\cdot\|$ can be used to measure how close a state is to the target state, i.e.:

$$d = \|x_T - x_6(u_k)\|, \quad (6)$$

where the notation $x_6(u_k)$ is used to emphasize the dependence of x_6 on u_k . Considering all possible input signals, one can compute the optimal control that finds the minimum distance for a given initial and target cell type. Let u_{*k} denote the optimal u_k used to minimize d , and d_* denotes this minimum distance value.

We note here that when determining which TFs can be used to reach x_T , it is often desirable and more experimentally feasible to minimize the number of distinct TFs given to the cells. Transfection of cells with multiple different TFs can lead to cell stress and death, and a lower efficiency of transfection overall. Moreover, many experimentally confirmed direct reprogramming regimes use ≤ 4 TFs to achieve reprogramming. For these reasons, we set all indices of u_k equal to zero, except for indices corresponding to TFs that we choose.

We define \hat{p} to be a set of positive integers that refer to the indices of u_k (read: TFs) that are allowed to be non-zero (e.g. $\hat{p} = \{1, 4, 7\}$ refers to TFs 1, 4, and 7). Let p be the number of elements in \hat{p} . Given a set of TFs (\hat{p}), we determine the quantity and timing of TF input (u_{*k}) that minimizes the difference (d_*) between the initial (x_I) and target (x_T) cell state. Mathematically, this can be written as

$$\begin{aligned}\underset{u_k}{\text{minimize}} \quad & \|x_T - x_6(u_k)\| \\ \text{subject to} \quad & \begin{cases} u_{m,k} \geq 0, & \text{if } m \in \hat{p} \\ u_{m,k} = 0, & \text{if } m \notin \hat{p} \end{cases}\end{aligned} \quad (7)$$

We use MATLAB's *lsqnonneg* function to solve Eq. 7, which gives u_{*k} and d_* .

Let $d_0 := \|x_T - x_I\|$, be the distance between initial and target states with no external influence. We define the score $\mu := d_0 - d_*$, which can be interpreted as the *distance progressed towards target*. μ can be calculated for each \hat{p} and sorted (high to low) to determine which TF or TF combination is the best candidate for direct reprogramming between x_I and x_T .

Remark: Subsets of TFs were chosen for each calculation based on the following criteria: ≥ 10 -fold expression increase in target state compared to initial state, and ≥ 4 RPKM in target state. These criteria are used to select differentially expressed TFs and TFs that are sufficiently active in the target state.

Results

Quantitative Measure Between Cell Types

In order to best utilize our algorithm to predict TFs for reprogramming, compatible data on target cell types must be collected. For this, we explore a number of publicly available databases where RNA-seq has been collected, along with RNA-seq data collected in our lab. The ENCODE Consortium has provided data on myotubes and embryonic stem cells (ESCs) (See SI) [16]. The GTEx portal provides RNA-seq data on a large variety of different human tissue types [17]. Although each GTEx experiment is performed on tissue samples, thus containing multiple different cell types, we use these data as more general cell state targets.

To give a numerical structure to cell type differences, conceptually similar to Waddington's epigenetic landscape, we calculate d_0 between all cell types collected. Fig. 3A shows d_0 values for 32 tissue samples collected from the GTEx portal, along with ESC, myotube, and our fibroblast data (additional cell type d_0 values shown in SI). Warmer colors (red) denote further distances

between cell types. GTEx RNA-seq data is scaled to keep total RPKM difference between time series fibroblast and GTEx fibroblast RNA-seq minimal (See SI).

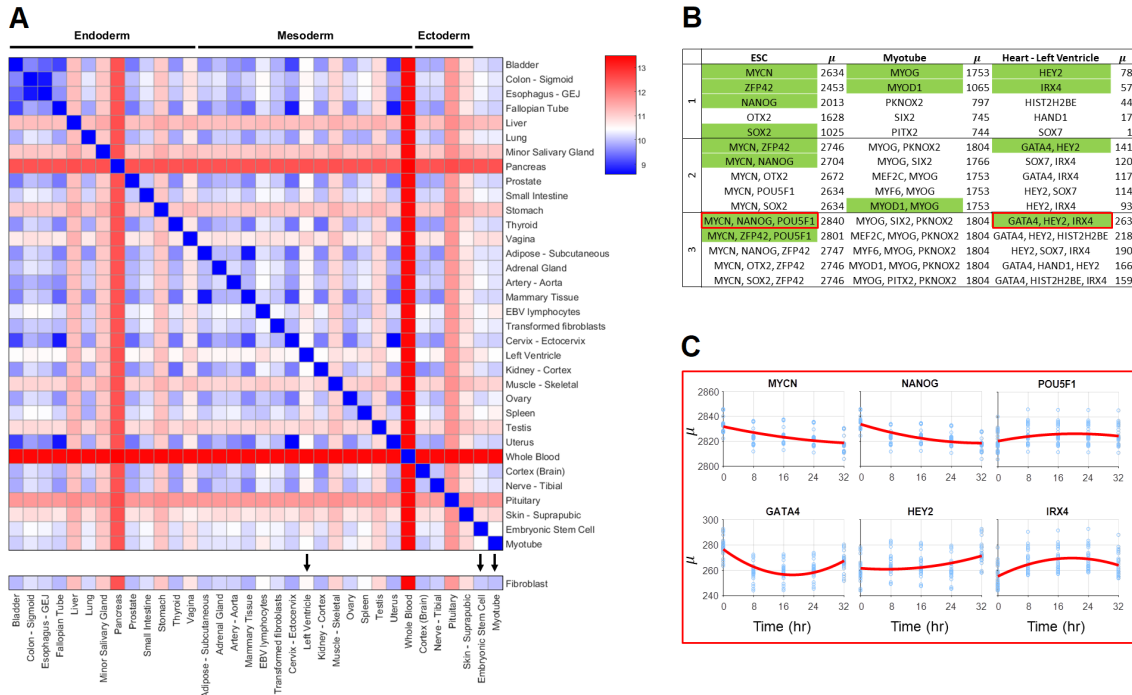


Figure 3: Quantitative measure between cell types and transcription factor scores. (A) d_0 values between GTEx tissue types and ESC, myotube, and fibroblast. Tissue types and cell types with black arrows have predicted transcription factors for reprogramming from fibroblasts shown in 3B. (B) Table of predicted transcription factors for a subset of cell and tissue types. Top 5 transcription factors for combinations of 1-3 shown. Green labeled transcription factors are either highly associated with the differentiation process of the target cell type and/or validated for reprogramming. These transcription factors are discussed in the main text. (C) Time-dependent scores for selected combinations of 3 transcription factors for fibroblast to ESC and fibroblast to "Heart - Left ventricle". x-axis refers to time of transcription factor addition, y-axis refers to μ .

TF Scores

To assess our method's predictive power, a subset of target cell types are presented here that have either validated TF reprogramming methods or TFs highly associated with the target cell type. Additional predicted TFs for reprogramming are included in SI. We note that though experimentally validated TFs provide the best current standard for comparison, we believe experimental validation with our predicted TFs may provide more efficient reprogramming results. For all reprogramming regimes presented in this section, fibroblast is used as the initial cell type due to the availability of synchronized time series data, and all TFs are introduced at $k = 1$ [9].

For conversion of fibroblast to myotubes, the top predicted single input TFs are MYOG and MYOD1, both of which are known to be crucial for myogenesis. While MYOD1 is the classic master regulator reprogramming TF for myotube conversion, activation of downstream factor MYOG is necessary for full conversion [18]. For fibroblast to ESC conversion, a number of TFs known to be necessary for pluripotency are predicted, including MYCN, ZFP42, NANOG, and SOX2 [19]. With the knowledge that no single TF has been shown to fully reprogram a fibroblast to an embryonic state, combinations of TFs are more informative for this analysis. The top scoring combination of 3 TFs is MYCN, NANOG, and POU5F1—three well-known markers for pluripotency [19]. Interestingly, POU5F1 scores poorly when input individually, but is within the top set of 3 TFs when used in combination with MYCN and NANOG. Left ventricle reprogramming includes TFs that are known to be necessary for natural differentiation in the top score for all 1-3 combinations.

These include GATA4 (a known TF in fibroblast to cardiomyocyte reprogramming), HEY2, and IRX4 [20, 21, 22].

Time-dependent TF Addition

Fibroblast to ESC conversion was of particular interest in our analysis as this is a well-studied regime with a number of validated TFs (with a variety of reported efficiencies), and this conversion is promising for its regenerative medicine application. High scoring TFs yield many that are known markers for pluripotency, but the top combination of 3, MYCN, NANOG, and POU5F1, has not been used specifically together, to our knowledge.

Since our method incorporates dynamical RNA-seq data, analysis can be extended to determine the best time to input control for a given set of TFs. In our model, there are five possible input times: 0, 8, \dots , 32 h. We assume a TF continues to influence the system at a constant value once input until the final time (40 h). We restrict our analysis here to combinations of 3 TFs. This gives $5^3 = 125$ possible *Time-dependent regimes* to input the TFs; e.g. $TF1, TF2, TF3$ are input, respectively, at times 0,0,0, or 0,0,8, or 0,0,16, or \dots or 32,32,24 or 32,32,32. Inputting a TF at time k^* can be viewed mathematically as requiring $u_{m,k} = 0$ for all $k < k^*$.

Time-dependent analysis of the top scoring ESC TFs reveals that scores vary widely depending on the time of input. MYCN and NANOG show a strong preference for input at the beginning of the cell cycle, while POU5F1 shows a slight preference for input towards the end of the cell cycle, with the highest score achieved when MYCN and NANOG are input at 0 h and POU5F1 is input at 32 h. Analysis on how the time of input control affects μ is shown in Fig. 3C. Time-dependent analysis was also conducted for the top combination of 3 TFs for fibroblast to left ventricle. This set includes GATA4, HEY2, and IRX4, all factors highly associated with the cardiac phenotype [20, 21, 22]. This analysis predicted that the best reprogramming results would occur if GATA4 is given immediately (0 h), with IRX4 and HEY2 given later (24 and 32 h, respectively).

Discussion

The results from this algorithm show promise in their prediction of known reprogramming TFs, and demonstrate the importance of including time series data for gene network dynamics. Time of input control has shown to have an impact on the end cell state, in line with what has been shown in natural differentiation [23].

While we believe that this is the best model currently available for predicting TFs for reprogramming, we are aware of its limitations and assumptions. TAD-based dimension reduction is based on the observation that genes within them correlate in expression over time, though we lack definitive proof of regulation by shared transcriptional machinery [9]. This assumption was deemed necessary for dimension reduction in the context of deriving transition matrix A_k . With finer time steps in RNA-seq data, the assumption may not be necessary for TF prediction, at the cost of increased computation time. Additionally, a 5kb window flanking the TSS of each gene was used to ensure that all potential regulators are found, at the cost of potential inclusion of false positive motifs.

GTEX data proved to be an invaluable resource for testing our algorithm, providing many target states for TF prediction. It is important to note that these data are collected from cadaver tissue samples; therefore the RNA-seq data is coming from a heterogeneous cell-type population and may be enriched for stress factors known to be elevated after death (e.g. HSF4). Ideally, RNA-seq data for target cells would be derived from a homogeneous population, with minimal experiment collection variables. Future work includes the extension of this DGC approach to other target cell types.

Although this program can score TFs relative to other TFs in a given reprogramming regime, it is difficult to predict a μ threshold that would guarantee conversion. Additionally, rigorous experimental testing will be required to validate these findings and determine how our u vector translates to TF concentration. This is a product of the large number of assumptions that must be made to develop the initial framework for a reprogramming algorithm. With finer resolution in the time series gene expression, more subtle aspects of the genomic network may be observed, allowing for better prediction.

Our proposed data-guided control framework successfully identified known TFs for fibroblast to ESC and fibroblast to muscle cell reprogramming regimes. The framework rates individual TFs

as well as sets of TFs. We employ a biologically-inspired dimension reduction via TADs, a natural partitioning of the genome. This comprehensive state representation was the foundation of our framework, and the success of our methods motivates further investigation of the importance of TADs as functional units to control the genome.

A dynamical systems view of the genome allows for analysis of timing, efficiency, and optimality in the context of reprogramming. Our framework is the first step toward this view. The successful implementation of time-varying reprogramming regimes would open new avenues for direct reprogramming. Experimental verification of predicted regimes and development of methods to identify optimal sets of TFs are planned for the near future. This template can be used to develop regimes for changing any cell into any other cell, for applications that include reprogramming cancer cells and controlling the immune system. Our DGC framework is well equipped for designing personalized cellular reprogramming regimes. Finally, this framework can serve as a general technique for investigating the controllability of networks strictly from data.

Methods and Materials

Hi-C and RNA-seq data were collected from cell cycle and circadian rhythm-synchronized proliferating human fibroblasts of normal karyotype. Data were collected every 8 h, spanning 56 h. Publicly available data was used for target cell types. Detailed materials and methods are provided in Chen *et al.* and in SI [9].

Acknowledgement

We thank Robert Oakes, Emily Crossette, and Sijia Liu for their critical reading of the manuscript and helpful discussions. We extend special thanks to James Gimlett and Srikanta Kumar at Defense Advanced Research Projects Agency (DARPA) for support and encouragement. This work is supported, in part, by the DARPA Biochronicity Program and the DARPA Deep-Purple and FunCC Program.

References

- [1] H. Weintraub, S.J. Tapscott, R.L. Davis, M.J. Thayer, M.A. Adam, A.B. Lassar, and A.D. Miller. Activation of muscle-specific genes in pigment, nerve, fat, liver, and fibroblast cell lines by forced expression of myod. *Proc. Natl. Acad. Sci. USA*, 86:5434–5438, 1989.
- [2] K. Takahashi, K. Tanabe, M. Ohnuki, M. Narita, T. Ichisaka, K. Tomoda, and S. Yamanaka. Induction of pluripotent stem cells from adult human fibroblasts by defined factors. *Cell*, 131(5):861–872, 2007.
- [3] R.W. Brockett. *Finite Dimensional Linear Systems*. John Wiley & Sons, Inc., New York, USA, 1970.
- [4] I. Rajapakse, M. Groudine, and M. Mesbahi. Dynamics and control of state-dependent networks for probing genomic organization. *PNAS*, 108:17257–17262, 2011.
- [5] G. Felsenfeld and M. Groudine. Controlling the double helix. *Nature*, 421:448–453, 2003.
- [6] O.J. Rackham, J. Firas, H. Fang, M.E. Oates, M.L. Holmes, A.S. Knaupp, FANTOM Consortium, H. Suzuki, C.M. Nefzger, C.O. Daub, J.W. Shin, E. Petretto, A.R. Forrest, Y. Hayashizaki, J.M. Polo, and J. Gough. A predictive computational framework for direct reprogramming between human cell types. *Nature genetics*, 2016.
- [7] Karl Johan Aström and Richard M Murray. *Feedback systems: an introduction for scientists and engineers*. Princeton university press, 2010.
- [8] Jesse R Dixon, Siddarth Selvaraj, Feng Yue, Audrey Kim, Yan Li, Yin Shen, Ming Hu, Jun S Liu, and Bing Ren. Topological domains in mammalian genomes identified by analysis of chromatin interactions. *Nature*, 485(7398):376–380, 2012.

- [9] Haiming Chen, Jie Chen, Lindsey A Muir, Scott Ronquist, Walter Meixner, Mats Ljungman, Thomas Ried, Stephen Smale, and Indika Rajapakse. Functional organization of the human 4d nucleome. *Proceedings of the National Academy of Sciences*, 112(26):8002–8007, 2015.
- [10] F. Ciabrelli and G. Cavalli. Chromatin-driven behavior of topologically associating domains. *Journal of Molecular Biology*, 427:608–625, 2015.
- [11] Jesse R Dixon, David U Gorkin, and Bing Ren. Chromatin domains: the unit of chromosome organization. *Molecular cell*, 62(5):668–680, 2016.
- [12] J. Chen, A. Hero, and I. Rajapakse. Spectral identification of topological domains. *Bioinformatics*, accepted 2016.
- [13] David S. Latchman. Transcription factors: an overview. *The international journal of biochemistry and cell biology*, 29.12:1305–1312, 1997.
- [14] Robert E Thurman, Eric Rynes, Richard Humbert, Jeff Vierstra, Matthew T Maurano, Eric Haugen, Nathan C Sheffield, Andrew B Stergachis, Hao Wang, Benjamin Vernot, et al. The accessible chromatin landscape of the human genome. *Nature*, 489(7414):75–82, 2012.
- [15] Robert C Brewster, Franz M Weinert, Hernan G Garcia, Dan Song, Mattias Rydenfelt, and Rob Phillips. The transcription factor titration effect dictates level of gene expression. *Cell*, 156(6):1312–1323, 2014.
- [16] ENCODE Project Consortium et al. An integrated encyclopedia of dna elements in the human genome. *Nature*, 489(7414):57–74, 2012.
- [17] John Lonsdale, Jeffrey Thomas, Mike Salvatore, Rebecca Phillips, Edmund Lo, Saboor Shad, Richard Hasz, Gary Walters, Fernando Garcia, Nancy Young, et al. The genotype-tissue expression (gtex) project. *Nature genetics*, 45(6):580–585, 2013.
- [18] Harold Weintraub. The myod family and myogenesis: redundancy, networks, and thresholds. *Cell*, 75(7):1241–1244, 1993.
- [19] Kazutoshi Takahashi, Koji Tanabe, Mari Ohnuki, Megumi Narita, Tomoko Ichisaka, Kiichiro Tomoda, and Shinya Yamanaka. Induction of pluripotent stem cells from adult human fibroblasts by defined factors. *cell*, 131(5):861–872, 2007.
- [20] Masaki Ieda, Ji-Dong Fu, Paul Delgado-Olguin, Vasanth Vedantham, Yohei Hayashi, Benoit G Bruneau, and Deepak Srivastava. Direct reprogramming of fibroblasts into functional cardiomyocytes by defined factors. *Cell*, 142(3):375–386, 2010.
- [21] Andreas Fischer, Nina Schumacher, Manfred Maier, Michael Sendtner, and Manfred Gessler. The notch target genes hey1 and hey2 are required for embryonic vascular development. *Genes & development*, 18(8):901–911, 2004.
- [22] Daryl O Nelson, Dexter X Jin, Karen M Downs, Timothy J Kamp, and Gary E Lyons. Irx4 identifies a chamber-specific cell population that contributes to ventricular myocardium development. *Developmental Dynamics*, 243(3):381–392, 2014.
- [23] Kyle M Loh, Angela Chen, Pang Wei Koh, Tianda Z Deng, Rahul Sinha, Jonathan M Tsai, Amira A Barkal, Kimberle Y Shen, Rajan Jain, Rachel M Morganti, et al. Mapping the pairwise choices leading from pluripotency to human bone, heart, and other mesoderm cell types. *Cell*, 166(2):451–467, 2016.
- [24] David Adams, Lucia Altucci, Stylianos E Antonarakis, Juan Ballesteros, Stephan Beck, Adrian Bird, Christoph Bock, Bernhard Boehm, Elias Campo, Andrea Caricasole, et al. Blueprint to decode the epigenetic signature written in blood. *Nature biotechnology*, 30(3):224–226, 2012.
- [25] S. Neph, A.B. Stergachis, A. Reynolds, R. Sandstrom, E. Borenstein, and J.A. Stamatoyannopoulos. Circuitry and dynamics of human transcription factor regulatory networks. *Cell*, 150:1274–1286, 2012.
- [26] P Shannon. Motifdb: An annotated collection of protein-dna binding sequence motifs. *R package version*, 1(0), 2014.

- [27] Maria A Jimenez, Peter Åkerblad, Mikael Sigvardsson, and Evan D Rosen. Critical role for ebf1 and ebf2 in the adipogenic transcriptional cascade. *Molecular and cellular biology*, 27(2):743–757, 2007.
- [28] Francine M Gregoire, Cynthia M Smas, and Hei Sook Sul. Understanding adipocyte differentiation. *Physiological reviews*, 78(3):783–809, 1998.
- [29] Min Kyung Jang, Cho Hee Kim, Je Kyung Seong, and Myeong Ho Jung. Atf3 inhibits adipocyte differentiation of 3t3-l1 cells. *Biochemical and biophysical research communications*, 421(1):38–43, 2012.
- [30] Takaki Miyata, Tomoko Maeda, and Jacqueline E Lee. Neurod is required for differentiation of the granule cells in the cerebellum and hippocampus. *Genes & development*, 13(13):1647–1652, 1999.
- [31] Christopher L Frank, Fang Liu, Ranjula Wijayatunge, Lingyun Song, Matthew T Biegler, Marty G Yang, Christopher M Vockley, Alexias Safi, Charles A Gersbach, Gregory E Crawford, et al. Regulation of chromatin accessibility and zic binding at enhancers in the developing cerebellum. *Nature neuroscience*, 18(5):647–656, 2015.
- [32] JS Cohen, S Srivastava, KD Farwell Hagman, DN Shinde, R Huether, D Darcy, R Wallerstein, G Houge, S Berland, KG Monaghan, et al. Further evidence that de novo missense and truncating variants in zbtb18 cause intellectual disability with variable features. *Clinical Genetics*, 2016.
- [33] Neeraja Sammeta, Debra L Hardin, and Timothy S McClintock. Uncx regulates proliferation of neural progenitor cells and neuronal survival in the olfactory epithelium. *Molecular and Cellular Neuroscience*, 45(4):398–407, 2010.
- [34] Kelli L VanDussen and Linda C Samuelson. Mouse atonal homolog 1 directs intestinal progenitors to secretory cell rather than absorptive cell fate. *Developmental biology*, 346(2):215–223, 2010.
- [35] Mary Ann S Crissey, Rong-Jun Guo, Shinsuke Funakoshi, Jianping Kong, Jesse Liu, and John P Lynch. Cdx2 levels modulate intestinal epithelium maturity and paneth cell development. *Gastroenterology*, 140(2):517–528, 2011.
- [36] Ann DeLaForest, Masato Nagaoka, Karim Si-Tayeb, Fallon K Noto, Genevieve Konopka, Michele A Battle, and Stephen A Duncan. Hnf4a is essential for specification of hepatic progenitors from human pluripotent stem cells. *Development*, 138(19):4143–4153, 2011.
- [37] Asha Seth, Jianming Ye, Nanjia Yu, Fanny Guez, David C Bedford, Geoffrey A Neale, Sabine Cordi, Paul K Brindle, Frederic P Lemaigre, Klaus H Kaestner, et al. Prox1 ablation in hepatic progenitors causes defective hepatocyte specification and increases biliary cell commitment. *Development*, 141(3):538–547, 2014.
- [38] Gregory B Vanden Heuvel, Jennifer G Brantley, Neal I Alcalay, Madhulika Sharma, Gabor Kemeny, Joshua Warolin, Aric W Ledford, and David M Pinson. Hepatomegaly in transgenic mice expressing the homeobox gene *cux-1*. *Molecular carcinogenesis*, 43(1):18–30, 2005.
- [39] Ru Feng, Sabrina C Desbordes, Huafeng Xie, Ester Sanchez Tillo, Fiona Pixley, E Richard Stanley, and Thomas Graf. Pu. 1 and *c/ebpa*/ β convert fibroblasts into macrophage-like cells. *Proceedings of the National Academy of Sciences*, 105(16):6057–6062, 2008.
- [40] Heiko Bruns, Dimitrios Mougiakakos, Christian Bach, Martin Böttcher, Joerg Thomas Bittenbring, Maike Büttner, Kolja Gelse, Michael Rehli, Julia Wimmer, Fabian Beier, et al. the *ikzf1-irf4* axis regulates macrophage polarization and macrophage-mediated anti-tumor immunity, 2016.
- [41] Elisa Gomez Perdiguero and Frederic Geissmann. The development and maintenance of resident macrophages. *Nature immunology*, 17(1):2–8, 2016.

- [42] Cécile Naudin, Aurore Hattabi, Fabio Michelet, Ayda Miri-Nezhad, Aissa Benyoucef, Françoise Pflumio, François Guillonnet, Serge Fichelson, Isabelle Vigon, Isabelle Dusanter-Fourt, et al. Pim1/foxp1 signaling drives expansion of hematopoietic stem/progenitor and leukemia cells. *Blood*, 129(18):2493–2506, 2017.
- [43] Kiran Batta, Magdalena Florkowska, Valerie Kouskoff, and Georges Lacaud. Direct reprogramming of murine fibroblasts to hematopoietic progenitor cells. *Cell reports*, 9(5):1871–1884, 2014.
- [44] LM Starnes, A Sorrentino, M Ferracin, M Negrini, E Pelosi, Clara Nervi, and C Peschle. A transcriptome-wide approach reveals the key contribution of nfi-a in promoting erythroid differentiation of human [cd34. sup.+] progenitors and cml cells. *Leukemia*, 24(6):1220–1224, 2010.
- [45] M.L. Whitfield, G. Sherlock, A.J. Saldanha, J.I. Murray, C.A. Ball, K.E. Alexander, J.C. Matese, C.M. Perou, M.M. Hurt, P.O. Brown, and D. Botstein. Identification of genes periodically expressed in the human cell cycle and their expression in tumors. *Molecular biology of the cell*, 13.6:1977–2000, 2002.

Supporting Information (SI)

Data

The fibroblast (FIB) data (Hi-C and RNA-seq) used for this application was originally collected and published in a paper by Chen *et al.* [9]. We refer the reader to this paper for a full description of technical protocols. Embryonic Stem Cell (ESC) and myotube (MT) data was downloaded from NCBI-GEO (GSE23316 ENCODE Caltech RNA-seq and GSE52529) [16]. 53 different tissue RNA-seq samples were downloaded from GTEx portal [17]. 51 different immune cell type RNA-seq samples were obtained from the BLUEPRINT Epigenome project [24].

Hi-C and Construction of TADs

We computed TAD boundaries from genome-wide chromosome conformation capture (Hi-C) data using an algorithm described in Chen *et al.* [12]. The algorithm was applied to averaged time series Hi-C data from proliferating human fibroblast (FIB) at 100 kilo-base pair (kb) resolution, which identified 2,562 TADs across all autosomal chromosomes (i.e. excluding Chromosomes X and Y). Of the 2,562 TADs, 317 contained no genes and were excluded from our analysis, leaving 2,245 TADs. These TADs ranged in size from a few hundred kb to several Mb, and contained on average 9-10 genes (standard deviation of 18 genes); one gene at minimum, and 249 genes maximum.

Construction of B Matrix

TF binding site position frequency matrix (PFM) information was obtained from Neph *et al.* and MotifDB, which is a collection of publicly available PFM databases such as, JASPAR, Jolma *et al.* cispb_1.02, stamLab, hPDI, UniPROBE [25, 26]. TRANSFAC PFM information was included as well. Motif scanning of the human reference genome (hg19) was performed using FIMO of the MEME suite, in line with methods established by Neph *et al.* [25]. DNase-seq information for human fibroblasts was derived from ENCODE for fibroblast (GSM1014531). If a narrow peak is found within the ± 5 kb of a gene TSS, the region is classified as open. TF function information was determined through an extensive literature search.

Scaling of RNA-seq

Due to differences in data collection procedures, the RNA-seq RPKM values obtained from the GTEx portal were of lower value, on average, compared to our fibroblast dataset, thus favoring repressor TFs for μ scoring. In order to account for this in our model, we scaled all GTEx RNA-seq data by a factor that solves the equation

$$\underset{\alpha}{\text{minimize}} \quad \|g_{FIB,UM} - \alpha g_{FIB,GTEX}\| \quad (8)$$

where $g_{FIB,UM}$ is the gene-level RNA-seq vector average of our fibroblast data, $g_{FIB,GTEX}$ is the gene-level RNA-seq vector of “Cells - Transformed fibroblasts” from the GTEx portal, and α is a scalar that solves this equation. For this data, $\alpha = 2.6113$ and all GTEx data used as a target state was scaled by this factor.

Removal of MicroRNA

MicroRNA were removed from this analysis due to their high variance in RPKM values and unpredictable function.

TF Scores - Additional GTEx Data

For fibroblast to Adipose-Subcutaneous, the highest scoring factor is EBF1, a known maintainer of brown adipocyte identity, and a known promoter of adipogenesis in fibroblasts [27]. The 2nd

highest scoring marker, PPARG, has been shown to be involved in adipose differentiation, and can be used individually to achieve reprogramming from fibroblasts [28]. Curiously, ATF3 is implicated here as being useful for adipocyte differentiation although its function has been shown to repress PPARG and stymie cell proliferation [29]. Upon further research using time dependent addition, ATF3 addition scores best when added towards the end of reprogramming process.

2 Brain tissue samples, Cerebellum and Hippocampus, both predict TFs necessary for natural differentiation. Interestingly, our algorithm select different TFs for each conversion, with factors linked specifically to each tissue. For Cerebellum, NEUROD1, has been shown to be required for granule cell differentiation, while ZIC1 and ZIC4 are both known to promote cerebellar-specific neuronal function [30, 31]. The top scoring combination of 3 TFs are all similarly known to be important in neurogenesis (NEUROD1, ZBTB18, UNCX) [32, 33]. Hippocampus TF scoring includes FOXG1 as the top predicted factor, a factor specifically needed in hippocampus development. OLIG2, FOXG1, and GPD1 are the top scoring set for hippocampus reprogramming, all of which have been shown to been necessary for hippocampus function.

Colon TF scoring finds known differentiation factor in natural colon secretory lineage development, ATOH1, as the highest scoring individual factor [34]. The top scoring combination of 2 TFs includes ATOH1 along with CDX2, another known factor necessary for full differentiation of colon cells, specifically small intestine maturation [35]. Liver cell reprogramming similarly finds known factors for differentiation in the top score of all 3 combinations: HNF4A, CUX2, PROX1 [36, 37, 38]. All factor play a role in correct development of hepatic progenitor cell-types and hepatic stem cells, the cell types just above in lineage differentiation.

TF Scores - BLUEPRINT Project Data

A number of immune cell types extracted from the BLUEPRINT Project revealed promising predicted TF results when fibroblast is used as the starting point [24]. d_0 values between cell types are shown in Fig. S4.

For fibroblast to macrophage direct reprogramming, a number of factors scoring highly in our algorithm are known to play a role in macrophage reprogramming or the differentiation. SPI1 (along with CEBPA) has been verified experimentally to reprogram fibroblasts into macrophage-like cells [39]. IKZF1 has been shown to be crucial for macrophage polarization via the IRF4/IRF5 pathway [40]. MYB has been shown to be crucial for the upstream cell type HSC [41].

For fibroblast to HSC direct reprogramming, the top scoring individual factor is highly associated with the target phenotype and has been shown to support HSC growth and regeneration [42]. ERG (in combination with GATA2, LMO2, RUNX1c, and SCL) is a confirmed reprogramming factor for fibroblast to HSC in mice [43].

For fibroblast to erythroblast reprogramming, ERG is a promising factor as it is required for the maintenance of the upstream cell type HSC [43]. NFIA is shown to promote the erythroid lineage from HSC differentiation [44].

Alternative Computation of u

Below is an example of how u can be computed without the constraint that $u_{k,m} \geq 0$. Assume $u_k := \bar{u}$ is constant for all t . Then

$$x_{k+1} = A_k x_k + B u_k. \quad (9)$$

can be written as

$$x_4 = A_3 A_2 A_1 x_1 + C \bar{u}, \quad (10)$$

where

$$C := A_3 A_2 B + A_3 B + B$$

We seek the control \bar{u} that minimizes the distance between $x(3)$ and the target x_T :

$$\min_{\bar{u}} \|x_T - A_3 A_2 A_1 x_1 - C \bar{u}\|. \quad (11)$$

We can see that an exact solution exists if

$$x_T - A_3A_2A_1x_1 \in \text{span}(C), \quad (12)$$

and is given by

$$A_3A_2A_1x_1 + C\bar{u} = x_T \quad (13)$$

$$C\bar{u} = x_T - A_3A_2A_1x_1 \quad (14)$$

$$\bar{u} = C^\dagger (x_T - A_3A_2A_1x_1), \quad (15)$$

where C^\dagger denotes the Moore-Penrose pseudoinverse of the matrix C , computed using the singular value decomposition of C . Even when Eqn (12) is not satisfied, it is well established that the control (15) solves (11).

Define

$$d = \left\| (I_N - CC^\dagger)(x_T - A_3A_2A_1x_1) \right\| \quad (16)$$

$$\mu := d_0 - d_* \quad (17)$$

μ can be used to compare between potential TFs for a defined initial state (x_I), target state (x_T), and TF number (p). The larger the value of μ , the higher the relative score for its corresponding TF set.

We note that accurate TF predictions for some desired target cell type may not depend on minimizing distance alone, but also the amount of "energy" required for the system to reach d_* . We denote energy here with μ_2 and define it as:

$$e(u) = \sum_{k=0}^{K-1} u_k^T \cdot u_k = \mu_2. \quad (18)$$

μ_2 is analogous to the amount of a TF that needs to be added to the system to achieve d_* . In the case where two different TFs achieve the same μ score, μ_2 can be computed to decide the better candidate (i.e. lower μ_2 is better TF).

SI Figures

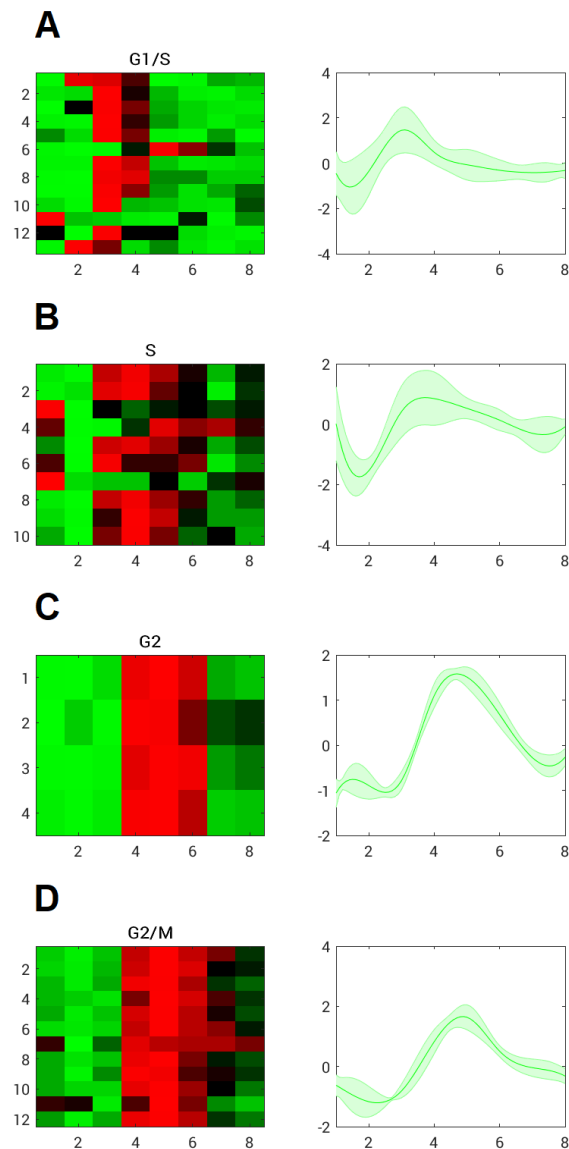


Figure S1: Analysis of cell cycle marker gene expression. Gene expression RNA-seq data for 39 genes that have been shown in the literature to be cell cycle regulated [45]. Cell cycle phases shown include (A) G_1/S , (B) S, (C) G_2 , (D) G_2/M . Raw data of gene expression over time (left), with smoothed/interpolated expression over time with standard deviation (right). The expression curves for each gene have been standardized by subtracting their mean and dividing by the standard deviation over the eight time points. x-axis denotes sample time point k , referring to 0, 8, 16, \dots , 56 h after growth medium introduction. y-axis is normalized expression.

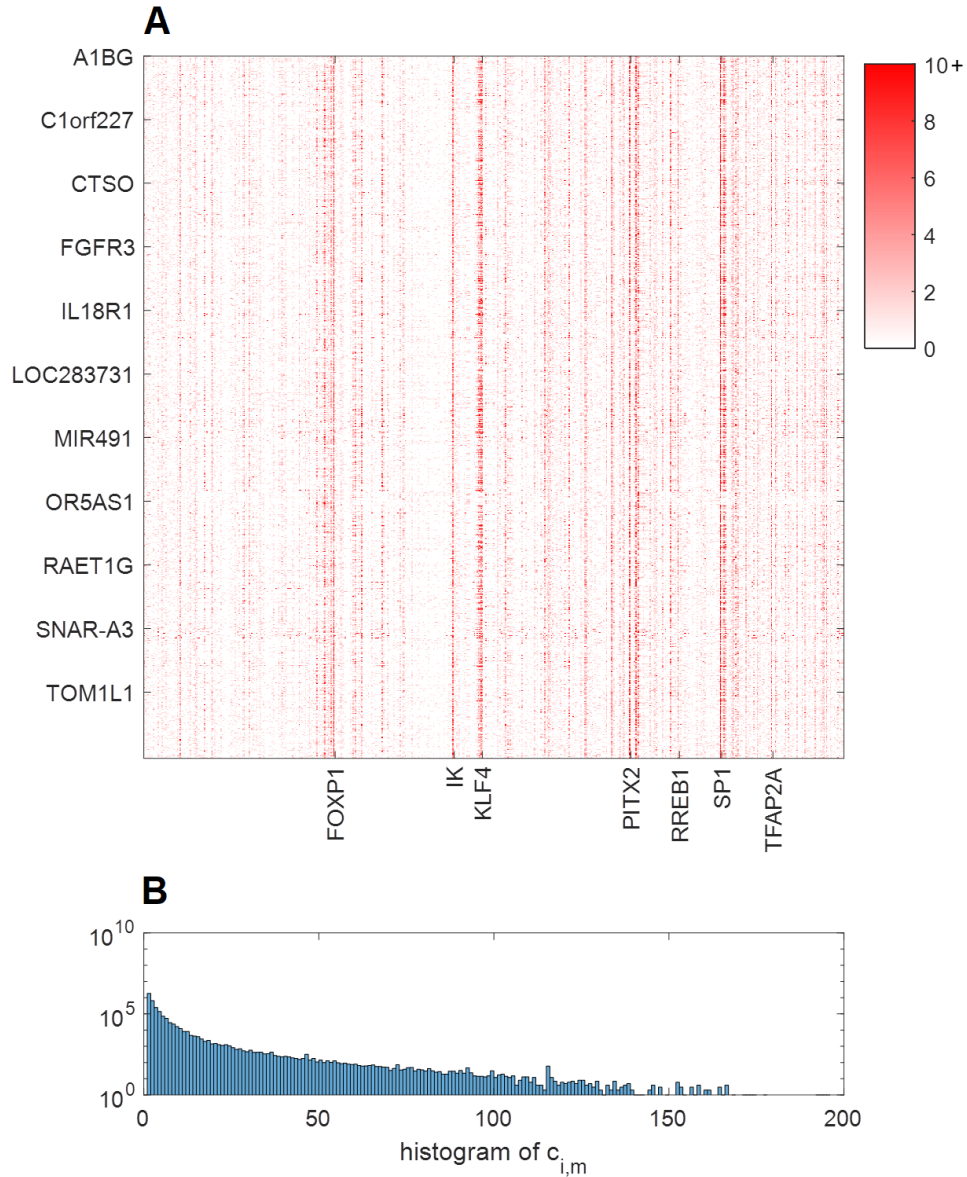


Figure S2: Visualization of input matrix **B**. (A) Visualization of the $22,083 \times 547$ $c_{i,m}$ matrix: identified TF-to-gene interactions based on TFBSs. The color at entry (i, m) represents how many transcription factor m TFBSs were observed within ± 5 kb of gene i 's TSS. The color axis has been truncated to $[0, 10]$ but note that more than 10 TFBSs were observed for many (gene,TF) pairs. Certain columns (TFs) are dramatically highlighted compared to others, some of which have been labeled by name along the horizontal axis. Some gene names are labeled along the vertical axis, none of which particularly stand out. Both genes and TFs are sorted alphabetically. (B) A histogram for the non-zero values of $c_{i,m}$. The log-scale on the vertical axis emphasizes that most of the gene TSS regions contain much less than 25 TFBSs for a given TF. The *SP1* TFBS, for example, is observed 249 times in a 10kb TSS centered on a gene.

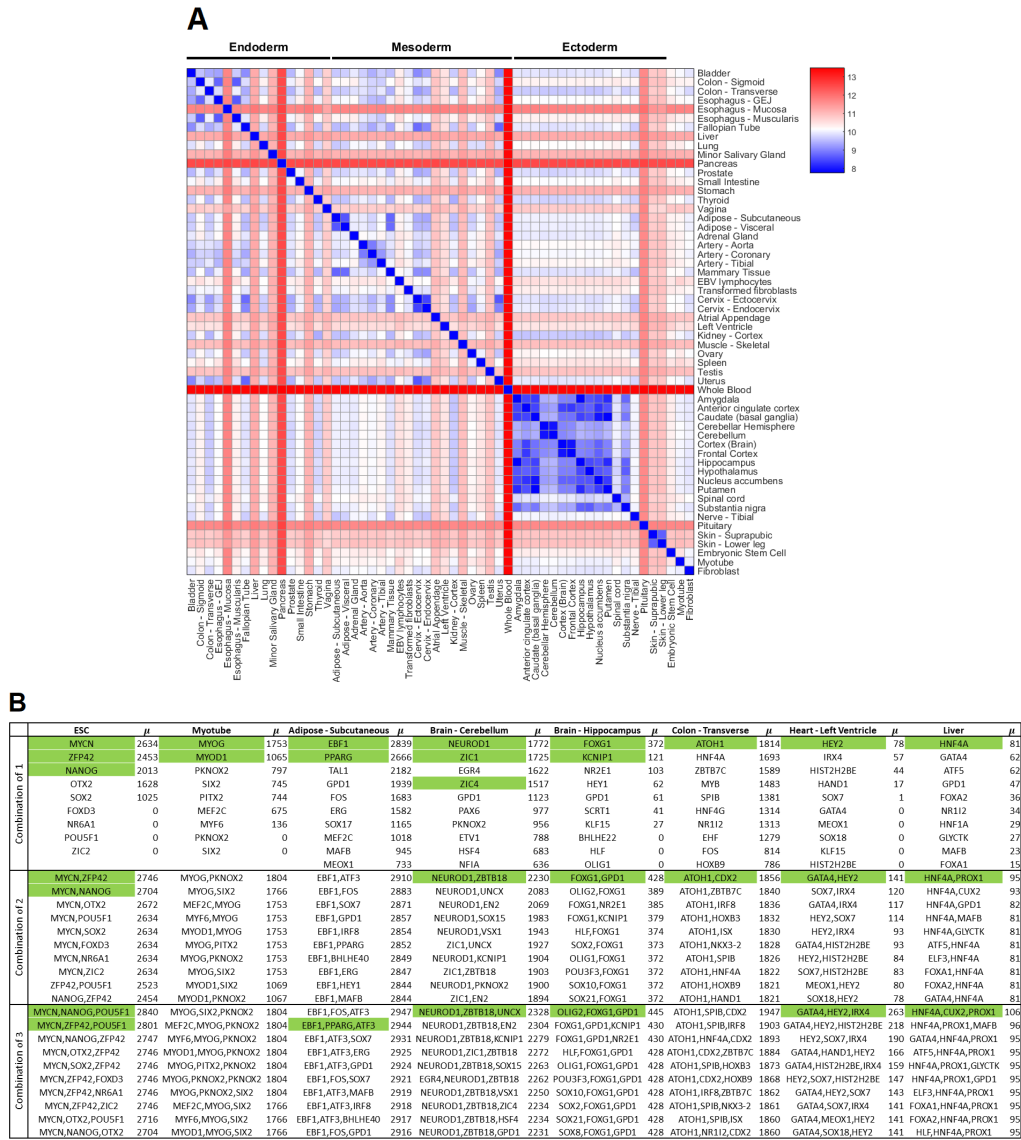
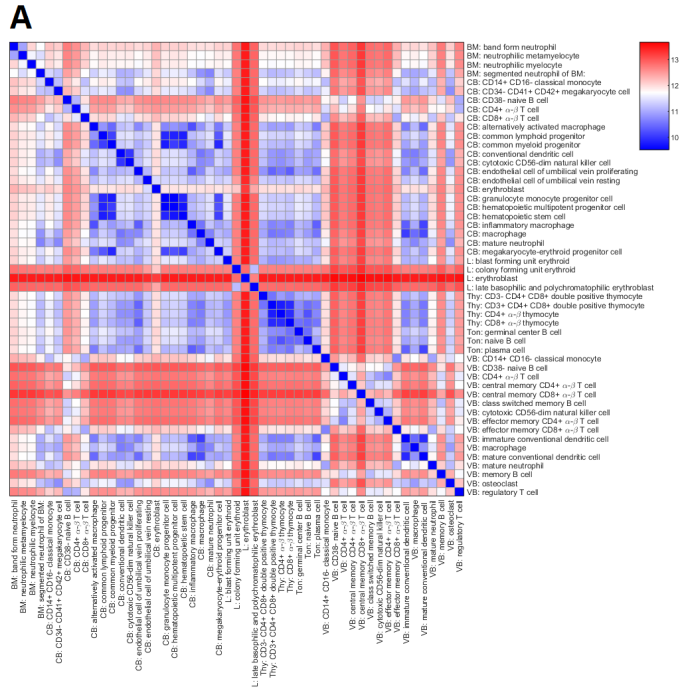


Figure S3: Quantitative measure between cell types and transcription factor scores. (A) d_0 values between all GTEx tissue types. (B) TF scores for an extended list of target cell types. $x_I =$ fibroblast



B

	Cord Blood - HSC	Cord Blood - HMPP	Cord Blood - Macrophage	Cord Blood - B cell	Cord Blood - Neutrophil	Cord Blood - Erythroblast	Cord Blood - Natural Killer cell	Cord Blood - Megakaryocyte cell								
Combination of 1	FOXP1	6304	FOXP1	5550	EHF	1724	FL11	5850	GZF1	2770	ERG	3915	MYBL1	1657	MYB	3363
	IKZF1	5704	HMBX1	4960	IKZF1	1705	REL	5768	MYB	2693	NFIA	3850	REL	833	FLI1	2691
	SP1	5568	IKZF1	4707	SP1	1568	RUNX3	5694	CREB5	2618	TFEC	3775	IKZF3	794	SP1	2618
	TAL1	5403	ERG	4427	MYB	1556	SP1	5393	FOXO3	2303	MYB	3611	RUNX3	737	IKZF3	2523
	ERG	5343	FL11	4352	BHLHE41	1485	PAX5	5209	ERG	2199	ATF3	3608	HMBX1	726	PAX5	2520
	HMBX1	5316	MYB	4291	ITGB2	1393	IKZF1	5095	REL	2198	LMO2	3493	ERG	713	IKZF1	2519
	MYB	5296	SOX4	4213	REL	1323	IKZF2	4977	SP1	2159	NFE2	3357	FL11	703	ITGB2	2470
	FL11	5221	ZNF350	4148	BATF	1256	HMBX1	4880	IKZF1	2136	IKZF1	3347	IKZF1	633	BATF	2457
	ITGB2	4918	LMO2	3900	TFEC	1206	ITGB2	4755	RUNX3	2126	TAL1	3346	BATF	614	SP1B	2380
	LMO2	4875	ITGB2	3811	LMO2	1116	TCF7	4655	BATF	1981	ITGB2	3176	IRF4	573	NFE2	2301
Combination of 2	FOXP1,HMBX1	6554	FOXP1,HMBX1	5877	IKZF1,LMO2	2052	FL11,HMBX1	6253	MYB,TAL1	3596	ERG,ZSCAN16	4139	IKZF2,MYBL1	2490	MYB,TAL1	4160
	ERG,FOXP1	6341	FOXP1,CHD2	5636	EHF,LMO2	1958	REL,HMBX1	6148	MYB,LMO2	3346	ERG,TFEC	4056	MYBL1,LMO2	2488	MYB,LMO2	3964
	SP11,FOXP1	6334	FOXP1,NFIA	5621	SP11,LMO2	1787	FL11,FOXP1	6071	CREB5,GZF1	3070	ERG,E2F2	4053	MYBL1,IKZF1	2443	MYB,IKZF1	3903
	FOXP1,CHD2	6325	FOXP1,SOX4	5604	IKZF1,TFEC	1772	HMBX1,RUNX3	6049	MYB,CHD2	3030	ERG,NFIA	4047	GF11,MYBL1	2174	MYB,GF11B	3680
	FL11,FOXP1	6324	FOXP1,TFEC	5590	IKZF1,ITGB2	1759	REL,FOXP1	5992	MYB,GZF1	2995	ERG,HMBX1	4035	MYBL1,ITGB2	2169	MYB,ITGB2	3674
	FOXP1,ZBTB16	6321	FOXP1,ZNF350	5590	EHF,IKZF1	1756	RUNX3,CHD2	5987	MYB,ITGB2	2975	NFIA,TFEC	4030	RORA,MYBL1	2096	MYB,TFEC	3600
	FOXP1,IKZF1	6318	FOXP1,ITGB2	5580	EHF,TFEC	1756	FL11,REL	5978	MYB,IKZF1	2936	NFIA,ZSCAN16	4026	MYBL1,RUNX3	2063	MYB,MEIS1	3566
	MYB,FOXP1	6316	FOXP1,LMO2	5568	EHF,ITGB2	1743	FL11,RUNX3	5943	MYB,GF11B	2923	ERG,E2F8	3993	MYBL1,ZBTB16	2036	MYB,ZBTB16	3459
	ITGB2,FOXP1	6313	FOXP1,IKZF1	5559	EHF,HMBX1	1732	FL11,TCF7	5927	MYB,RUNX3	2910	ERG,ITGB2	3945	BC168,MYBL1	1966	MYB,HMBX1	3382
	FOXP1,TAL1	6312	FOXP1,ZBTB16	5554	BHLHE41,EHF	1728	FL11,CHD2	5927	CREB5,MYB	2833	ATF3,ERG	3941	NFIB,MYBL1	1925	MYB,IKZF3	3372
Combination of 3	FOXP1,HMBX1,ZBTB16	6713	FOXP1,HMBX1,SOX4	6197	EHF,IKZF1,LMO2	2243	FL11,HMBX1,FOXP1	7071	MYB,GZF1,TAL1	4151	ATF3,ERG,E2F2	4504	MYBL1,ZBTB16,LMO2	2717	MYB,GF11B,LMO2	4282
	FOXP1,HMBX1,HMBX1	6600	FOXP1,HMBX1,ZBTB16	6005	BHLHE41,IKZF1,LMO2	2142	REL,HMBX1,FOXP1	6882	CREB5,MYB,TAL1	4051	ERG,NFIA,ZSCAN16	4457	IKZF2,MYBL1,LMO2	2717	MYB,GF11B,TAL1	4246
	ERG,FOXP1,HMBX1	6576	FOXP1,NFIA	5984	EHF,MYB,LMO2	2083	HMBX1,RUNX3,FOXP1	6614	MYB,CHD2,TAL1	3825	ERG,TFEC,E2F2	4435	IKZF2,MYBL1,HMBX1	2675	MYB,IKZF1,TAL1	4240
	SP11,FOXP1,CHD2	6576	FOXP1,HMBX1,ZNF350	5969	MYB,IKZF1,LMO2	2083	FL11,TCF7,FOXP1	6563	FOXO3,MYB,TAL1	3783	ERG,TFEC,ZSCAN16	4406	MYBL1,IKZF1,ZBTB16	2603	MYB,ITGB2,TAL1	4219
	MEIS1,FOXP1,HMBX1	6575	FOXP1,HMBX1,CHD2	5953	IKZF1,LMO2,ZBTB16	2078	SP11,HMBX1,FOXP1	6457	MYB,GZF1,LMO2	3747	ERG,NFIA,E2F2	4364	MYBL1,IKZF1,LMO2	2564	MYB,LMO2,TAL1	4204
	FOXP1,HMBX1,CHD2	6572	MEIS1,FOXP1,HMBX1	5948	ERG,IKZF1,LMO2	2072	FL11,HMBX1,IKZF1	6398	CREB5,MYB,LMO2	3720	NFIA,TFEC,ZSCAN16	4354	IKZF2,MYBL1,IKZF1	2562	MYB,TAL1,TFEC	4201
	FL11,FOXP1,HMBX1	6566	FOXP1,HMBX1,BKX	5937	BHLHE41,EHF,LMO2	2070	FL11,REL,FOXP1	6391	MYB,ZBTB16,TAL1	3649	ATF3,NFIA,E2F2	4324	BC168,MYBL1,LMO2	2560	MYB,IKZF3,TAL1	4192
	SP11,FOXP1,HMBX1	6565	FOXP1,HMBX1,TFEC	5915	IKZF1,ITGB2,LMO2	2068	FL11,IKZF3,FOXP1	6374	MYB,LMO2,TAL1	3635	NFIA,TFEC,E2F2	4286	GF11,MYBL1,LMO2	2559	MYB,IKZF1,LMO2	4179
	ITGB2,FOXP1,HMBX1	6564	FOXP1,HMBX1,ITGB2	5906	SP11,IKZF1,LMO2	2064	FL11,RUNX3,CHD2	6344	MYB,ITGB2,TAL1	3633	ERG,MYB,ZSCAN16	4272	IKZF2,MYBL1,ITGB2	2558	MYB,HMBX1,TAL1	4168
	FOXP1,HMBX1,NFIA	6560	FOXP1,HMBX1,LMO2	5904	IKZF1,HMBX1,LMO2	2052	RUNX3,CHD2,FOXP1	6332	MYB,GF11B,TAL1	3630	ATF3,MYB,E2F2	4263	REL,MYBL1,LMO2	2548	MYB,TAL1,ZBTB16	4164

Figure S4: Quantitative measure between cell types and TF scores for BLUEPRINT Project database. (A) d_0 values between BLUEPRINT Project cell types. (B) TF scores for an extended list of target cell types. x_I = fibroblast